A Discontinuous Galerkin Augmented Electric Field Integral Equation for Multiscale Electromagnetic Scattering Problems

Yibei Hou, *Student Member, IEEE*, Gaobiao Xiao, *Member, IEEE*, and Xuezhe Tian, *Member, IEEE*

***Abstract*— A discontinuous Galerkin (DG) augmented electric field integral equation method based on the domain decomposition is proposed in this paper for full-wave solution of multiscale targets. The conventional surface integral equation-based DG method allowing both conformal and nonconformal discretizations for multiscale structures suffers from low-frequency breakdown. By augmenting the DG-EFIE with current continuity equation, the proposed scheme can alleviate the low-frequency breakdown. In the augmented system, the electric field integral equation and the current continuity equation are discretized by using hybrid basis functions including Rao–Wilton–Glisson (RWG) and half RWG basis functions. Since the half RWG basis is not divergence conforming, line charge degrees of freedom on the adjoining edges are introduced in this paper. It is observed that the resulting linear system is well conditioned at low frequencies, which leads to a rapid convergence over wide frequency band. Numerical examples demonstrate the accuracy and efficiency of the augmented system.**

***Index Terms*— Augmented electric field integral equation (AEFIE), discontinuous Galerkin (DG), low frequency, multiscale targets.**

I. Introduction

SURFACE integral equation (SIE) [1]–[4] formulations provide a convenient technique for analyzing time-harmonic electromagnetic problems. Although volume integral equation can be used to solve electromagnetic problems, it requires volume discretization and the number of unknowns is large. When the perfectly electrical conducting (PEC) structures are studied, the magnetic field integral equation and the combined field integral equation cannot be used to model open structures, while the electric field integral equation (EFIE) can do. The EFIE is very popular in computational electromagnetic community because of its excellent accuracy. Usually, div-conforming basis functions, for example, the Rao–Wilton–Glisson (RWG) basis functions [1], are chosen as test and trial basis functions for the EFIE. Consequently, the normal continuity of the surface current is enforced automatically. Since each RWG basis function is defined on a pair of adjacent triangles, the mesh is required to be conformal. However, it is time consuming to generate a conformal discretization for the multiscale targets where large frames and fine features coexist. For the multiscale objects, it is apparent that we can first divide the targets into several subdomains according to the domain decomposition [5]–[7] concept, and generate the mesh of every parts independently. Unfortunately, nonconformal discretization is well encountered along the tearing lines between adjacent subdomains.

In the effort devoted to handling nonconformal meshes, discontinuous Galerkin (DG) methods [8]–[10] have received much attention recently. From the perspective of DG, the normal continuity is weakly enforced and the discontinuity is allowed along the contours. DG has been very popular with finite-element method, especially the DG time domain which is widely used for solving electromagnetic problems such as scattering problems [11]–[13], integrated circuit systems [14]–[16], and so on. Recently, DG-SIE method [17], [18] has been proposed to extend the DG method to SIEs for electromagnetic scattering problems. The main difficulty of the combination of DG and SIE, especially the EFIE, is to handle the normal discontinuity of the currents across boundary contour. The DG-SIE method shows great flexibility in the mesh preparation and local refinement.

EFIE suffers from the low-frequency breakdown [4], [19]–[24] due to the decoupling of the fields produced by electric currents and charges at low frequencies. When the simulation frequency decreases, the EFIE impedance matrix becomes increasingly ill conditioned and hence is hard to be solved accurately and efficiently. There are several approaches existing for overcoming the low-frequency breakdown of the EFIE. Quasi-Helmholtz decomposition-based methods, such as loop-star (LS) [19], [20] and loop-tree (LT) [4] decomposition, separate the current into divergence-free current and nondivergence-free current; hence, the conditioning is improved at low frequencies. However, it is difficult to employ the quasi-Helmholtz decomposition adopting half RWG basis functions in DG-EFIE. The augmented EFIE (AEFIE) [2], [3], [25]–[27] offers an attractive way to renormalize the EFIE and hence eliminates the low-frequency breakdown without searching for LS/LT basis functions. Although the above methods are efficient for low-frequency problems, they cannot handle multiscale targets with nonconformal discretization.

Manuscript received July 5, 2016; revised February 13, 2017; accepted April 22, 2017. Date of publication May 9, 2017; date of current version July 1, 2017. This work was supported in part by the National Science Foundation of China under Grant 61234001 and in part by the SAST Foundation under Grant 804-201505. *(Corresponding author: Yibei Hou.)*

Y. Hou and G. Xiao are with the Key Laboratory of Ministry of Education of Design and Electromagnetic Compatibility of High-Speed Electronic Systems, Shanghai Jiao Tong University, Shanghai 200240, China (e-mail: yibhou@sjtu.edu.cn; gaobiaoxiao@sjtu.edu.cn).

X. Tian is with the ElectroScience Laboratory, Electrical and Computer Engineering Department, Ohio State University, Columbus, OH 43212 USA (e-mail: tian.361@osu.edu).

Color versions of one or more of the figures in this paper are available online at http://ieeexplore.ieee.org.

Digital Object Identifier 10.1109/TAP.2017.2702716

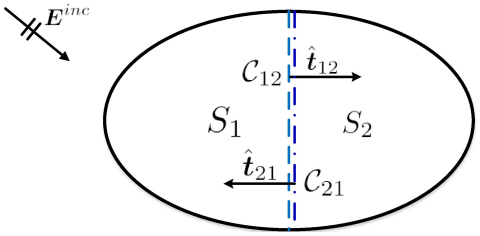

Fig. 1. Electromagnetic plane wave scattering from a PEC structure, whose surface is decomposed into two parts.

In this paper, the DG-EFIE is augmented by current continuity equation [2]; hence, the DG-AEFIE formulation is introduced for the full-wave analysis of multiscale structures with nonconformal meshes. The DG-AEFIE based on domain decomposition concept is nonconformal in nature, allowing local mesh refined. The continuity of currents across the interfaces between neighboring domains is weakly enforced via DG scheme. On the nonconformal meshes along the interfaces between adjacent subdomains, half RWG basis functions are defined while RWG basis functions are defined elsewhere.

Our work and the method in [28], based on DG and AEFIE, aim to solve the multiscale problems with nonconformal meshes over wide frequency range. However, our approach is different from [28] in the following aspects. First, our method introduces line charge to represent the discontinuity of the normal current across the contour interface. With the aid of line and surface charge, the current continuity equation can be properly implemented at the interfaces between adjacent subdomains. Second, the proposed DG-AEFIE does not move the line-face integral of the scalar term to the vector term. We separate the vector term and scalar term by adding surface and line charges to the unknown; consequently, the imbalance inherited from the conventional EFIE can be avoided. Third, charge neutrality is enforced to remove rank deficiency of the DG-AEFIE at low frequencies. Finally, the proposed scheme is well conditioned over frequencies and efficient for nonconformal meshes. It is worth noting that the term *low frequencies* refers to the case that the simulated structure is smaller than a wavelength. With the proposed method, both the conformal and the nonconformal mesh can be handled with great flexibility.

This paper is organized as follows. Section II introduces the formulation of DG-AEFIE and the associated perturbation method. In addition, preconditioning for DG-AEFIE is described. In Section III, several numerical examples are shown to validate the accuracy and the efficiency of the proposed method. Finally, some concluding remarks are summarized in Section IV.

II. Discontinuous Galerkin Augmented Electric Field Integral Equation

A. Formulation of DG-AEFIE

Consider a plane wave scattering from a PEC structure in Fig. 1 where the structure is divided into two parts. For simplicity, we assume the surface of the PEC structure S and its decomposition $S = S_1 \cup S_2$. In addition, we define the interior contour of S_i between S_i and S_j as $\mathcal{C}_{ij}$. The vector $\hat{\boldsymbol{t}}_{ij}$ stands for the outward-directed on-plane unit vector of the contour, which points from S_i to S_j. By relating the incident electromagnetic field $\boldsymbol{E}^{\text{inc}}$ to scattered field generated by the surface current $\boldsymbol{J}$, the EFIE can be written as

$$\hat{\boldsymbol{n}} \times jk_0 \int_S \left(1 + \frac{1}{k_0^2}\nabla\nabla\cdot\right) \boldsymbol{J}(\boldsymbol{r}')G(\boldsymbol{r},\boldsymbol{r}')dS' = \frac{1}{\eta_0}\hat{\boldsymbol{n}} \times \boldsymbol{E}^{\text{inc}}(\boldsymbol{r}) \tag{1}$$

where $\hat{\boldsymbol{n}}$ is the normal vector of the PEC surface S, k_0 and η_0 denote the free-space wave number and impedance, respectively, and $G(\boldsymbol{r},\boldsymbol{r}') = e^{-jk_0|\boldsymbol{r}-\boldsymbol{r}'|}/4\pi|\boldsymbol{r}-\boldsymbol{r}'|$ denotes the free-space Green's function. The PEC surface S is discretized into N_S triangles $(T_i, i = 1,\ldots,N_S)$ and N_E inner edges. The surface current is expanded by hybrid basis functions

$$\boldsymbol{J}(\boldsymbol{r}) = \sum_{m=1}^{N_R} j_{Rm}\boldsymbol{f}_m^R(\boldsymbol{r}) + \sum_{n=1}^{N_H} j_{Hn}\boldsymbol{f}_n^H(\boldsymbol{r}) \tag{2}$$

where $f_m^R((\boldsymbol{r})), m = 1,\ldots,N_R$, and $f_n^H((\boldsymbol{r})), n = 1,\ldots,N_H$, are modified RWG basis and modified half RWG basis without the edge length normalization [2], [25], [26] in this paper. N_R and N_H are the number of RWG basis functions and half RWG basis functions, respectively. The RWG basis is defined on a pair of triangles of S_i, while the half RWG basis is defined on the triangle along the contour $\mathcal{C}_{ij}$. It should be noted here that the interface meshes on S_i and S_j allow to be conformal and nonconformal.

The RWG basis is divergence conforming [1], [2], while the half RWG is not divergence conforming since there is additional part on the reference edge in the divergence formulation of the half RWG

$$\nabla\cdot\boldsymbol{f}_n^H(\boldsymbol{r}) = \begin{cases} \dfrac{1}{A_i} - \delta(\boldsymbol{r}-\boldsymbol{r}_{L_i})/l_i, & \boldsymbol{r}\in T_i \\ 0, & \text{otherwise} \end{cases} \tag{3}$$

in which $\boldsymbol{f}_n^H(\boldsymbol{r})$ is defined on the triangle whose area is A_i; in addition, L_i denotes the reference edge of $\boldsymbol{f}_n^H(\boldsymbol{r})$ and its length is l_i. Besides the current basis functions, charge basis functions including surface charge basis functions and line charge basis functions are also defined in this method. The surface charge basis

$$h_i^s(\boldsymbol{r}) = \begin{cases} \dfrac{1}{A_i}, & \boldsymbol{r}\in T_i \\ 0, & \text{otherwise} \end{cases} \tag{4}$$

is defined on the triangle T_i. For each edge CL_n, $n = 1,\ldots,N_L$, along the interface line between adjacent subdomains, we define the line charge basis as

$$h_n^l(\boldsymbol{r}) = \begin{cases} \delta(\boldsymbol{r}-\boldsymbol{r}_{CL_n}), & \boldsymbol{r}\in CL_n \\ 0, & \text{otherwise.} \end{cases} \tag{5}$$

For instance, the interface mesh on two subdomains is nonconformal in Fig. 2 and there are $N_L = 6$ line charge basis functions on the contour line. With the aid of the charge basis, the divergence of RWG basis can be expressed by

$$\nabla\cdot\boldsymbol{f}_m^R(\boldsymbol{r}) = \sum_{i=1}^{N_S} \overline{D}_{im}^{RS} h_i^s(\boldsymbol{r}) \tag{6}$$

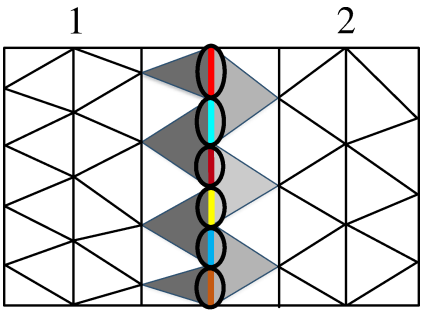

Fig. 2. Half RWG basis functions are defined on the triangles (gray) along the interface contour. There are six line charge basis functions (inside the black ring) placed on the contour line.

with

$$[\overline{D}^{\mathrm{RS}}]_{im} = \begin{cases} 1, & T_i \text{ is the positive triangle of } \boldsymbol{f}_m^R \\ -1, & T_i \text{ is the negative triangle of } \boldsymbol{f}_m^R \\ 0, & \text{otherwise.} \end{cases} \tag{7}$$

The divergence of half RWG basis functions can be given by

$$\nabla \cdot \boldsymbol{f}_m^H(\boldsymbol{r}) = \sum_{i=1}^{N_S} \overline{D}_{im}^{\mathrm{HS}} h_m^s(\boldsymbol{r}) + \sum_{n=1}^{N_L} \overline{D}_{nm}^{\mathrm{HL}} h_n^l(\boldsymbol{r}) \tag{8}$$

in which the matrix $\overline{\boldsymbol{D}}^{\mathrm{HS}} \in \mathbb{R}^{N_S \times N_H}$ is similar to the matrix $\overline{\boldsymbol{D}}^{\mathrm{RS}} \in \mathbb{R}^{N_S \times N_R}$ which links the current basis and the charge basis. The element of matrix $\overline{\boldsymbol{D}}^{\mathrm{HL}} \in \mathbb{R}^{N_L \times N_H}$ can be given by

$$[\overline{D}^{\mathrm{HL}}]_{nm} = \begin{cases} \dfrac{-1}{l_m}, & h_n^l \text{ is on the reference edge of } \boldsymbol{f}_m^H \\ 0, & \text{otherwise} \end{cases} \tag{9}$$

where l_m is the length of the reference edge of $\boldsymbol{f}_m^H$.

In the DG-SIE method [5], [17], [18], the test basis space is allowed to be discontinuous across the interface contours between adjacent subdomains. In our work, both the RWG basis and half RWG basis are chosen as testing basis and the EFIE (1) can be converted into matrix form

$$\left(jk_0 \widetilde{\boldsymbol{V}} + \frac{1}{jk_0} \widetilde{\boldsymbol{D}}^T \cdot \widetilde{\boldsymbol{P}} \cdot \widetilde{\boldsymbol{D}} \right) \cdot \boldsymbol{j} = \eta_0^{-1} \boldsymbol{b}. \tag{10}$$

The vector potential matrix $\widetilde{\boldsymbol{V}} \in \mathbb{C}^{(N_R+N_H)\times(N_R+N_H)}$ can be written by

$$\widetilde{\boldsymbol{V}} = \begin{bmatrix} \overline{\boldsymbol{V}}^{\mathrm{RR}} & \overline{\boldsymbol{V}}^{\mathrm{RH}} \\ \overline{\boldsymbol{V}}^{\mathrm{HR}} & \overline{\boldsymbol{V}}^{\mathrm{HH}} \end{bmatrix} \tag{11}$$

where

$$[\overline{V}^{\mathrm{RH}}]_{mn} = \int_{S_m} \boldsymbol{f}_m^R(\boldsymbol{r}) \cdot \int_{S_n} \boldsymbol{f}_n^H(\boldsymbol{r}') G(\boldsymbol{r}, \boldsymbol{r}') d\boldsymbol{S}' d\boldsymbol{S}. \tag{12}$$

The rest three submatrices in (11) can be obtained by changing the trial and test functions in (12). The sparse matrix $\widetilde{\boldsymbol{D}} \in \mathbb{R}^{(N_S+N_L)\times(N_R+N_H)}$ is given by

$$\widetilde{\boldsymbol{D}} = \begin{bmatrix} \overline{\boldsymbol{D}}^{RS} & \overline{\boldsymbol{D}}^{\mathrm{HS}} \\ \overline{\boldsymbol{0}} & \overline{\boldsymbol{D}}^{\mathrm{HL}} \end{bmatrix}. \tag{13}$$

The patch-line-based scalar potential matrix $\widetilde{\boldsymbol{P}} \in \mathbb{C}^{(N_S+N_L)\times(N_S+N_L)}$ denotes the coupling between any two charge basis functions

$$\widetilde{\boldsymbol{P}} = \begin{bmatrix} \overline{\boldsymbol{P}}^{\mathrm{SS}} & \overline{\boldsymbol{P}}^{\mathrm{SL}} \\ \overline{\boldsymbol{P}}^{\mathrm{LS}} & \overline{\boldsymbol{P}}^{\mathrm{LL}} \end{bmatrix} \tag{14}$$

in which the matrix $\overline{\boldsymbol{P}}^{\mathrm{SS}} \in \mathbb{C}^{(N_S \times N_S)}$ is the same as [2, eq. (3)]. The other matrix elements are

$$[\overline{P}^{\mathrm{SL}}]_{mn} = \int_{S_m} h_m^s(\boldsymbol{r}) \int_{L_n} h_n^l(\boldsymbol{r}') G(\boldsymbol{r}, \boldsymbol{r}') dL' dS \tag{15}$$

$$[\overline{P}^{\mathrm{LL}}]_{mn} = \int_{L_m} h_m^l(\boldsymbol{r}) \int_{L_n} h_n^l(\boldsymbol{r}') G(\boldsymbol{r}, \boldsymbol{r}') dL' dL. \tag{16}$$

The entries in $\overline{\boldsymbol{P}}^{\mathrm{LS}} \in \mathbb{C}^{N_L \times N_S}$ can be similarly computed by exchanging the inner and outer basis functions in (15). For (16), it becomes infinitely large when the observation point is located in the source line. Similar to the DG approach in [17], we add a boundary term $-\int_{L_m} h_m^l(\boldsymbol{r}) \int_{L_n} h_n^l(\boldsymbol{r}) G(\boldsymbol{r}, \boldsymbol{r}') dL' dL$ to the right-hand side in (16). It is noted that this boundary term will vanish. In order to weakly enforce the normal continuity of the current across the subdomain boundaries, we add an interior penalty (IP) [17] term to the line-based scalar potential matrix $\overline{\boldsymbol{P}}^{\mathrm{LL}} \in \mathbb{C}^{N_L \times N_L}$. Hence, the element of the matrix $\overline{\boldsymbol{P}}^{\mathrm{LL}}$ can be rewritten by

$$[\overline{P}^{\mathrm{LL}}]_{mn} = \beta \int_{\mathcal{C}_{mn}} \int_{\mathcal{C}_{mn}} h_m^l(\boldsymbol{r}) h_n^l(\boldsymbol{r}') / l_n' dL' dL \tag{17}$$

where l_n' denotes the length of the domain of h_n^l and β is the IP stabilization function, which is taken as $\beta = \alpha h^{-1}$. Here, h is the average length of mesh edges while the stabilization parameter α is positive and can be chosen as $20\log(\lambda/h)$. Since the integration domain in (17) is the common region between h_m^l and h_n^l, $\overline{P}_{mn}^{\mathrm{LL}}$ equals zero when m does not equal n.

In [5], [17], and [18], the DG-EFIE shows great flexibility and high efficiency to analyze multiscale targets. However, as the frequency decreases, the scalar term overwhelms the vector term and the conditioning becomes worse. Hence, it is hard to solve DG-EFIE accurately and efficiently at low frequencies. By augmenting the DG-EFIE with current continuity equation [2], the conditioning of DG-EFIE can be improved. The current continuity equation is discretized as

$$\widetilde{\boldsymbol{D}} \cdot \boldsymbol{j} = -j\omega \boldsymbol{\rho} \tag{18}$$

where the vector $\boldsymbol{j} \in \mathbb{C}^{(N_R+N_H)\times 1}$ stands for the coefficients of RWG and half RWG basis functions and the vector $\boldsymbol{\rho} \in \mathbb{C}^{(N_S+N_L)\times 1}$ denotes the coefficients of surface and line charge basis functions. Combining (10) and (18), we can obtain the formulation of DG-AEFIE

$$\begin{bmatrix} \widetilde{\boldsymbol{V}} & \widetilde{\boldsymbol{D}}^T \cdot \widetilde{\boldsymbol{P}} \\ \widetilde{\boldsymbol{D}} & k_0^2 \widetilde{\boldsymbol{I}} \end{bmatrix} \cdot \begin{bmatrix} jk_0 \boldsymbol{j} \\ c_0 \boldsymbol{\rho} \end{bmatrix} = \begin{bmatrix} \eta_0^{-1} \boldsymbol{b} \\ \boldsymbol{0} \end{bmatrix} \tag{19}$$

where the dimension of identity matrix $\widetilde{\boldsymbol{I}}$ is $N_S + N_R$.

Charge neutrality [2] is applied to avoid the rank deficiency of (19) at low frequencies. A charge unknown should be dropped from each unattached object; hence, the charge coefficient vector is reduced to be $\boldsymbol{\rho}_r \in \mathbb{C}^{(N_S+N_R-t)\times 1}$,

where t stands for the number of disconnected objects. Here, two mapping matrices $\widetilde{\boldsymbol{F}} \in \mathbb{R}^{(N_S+N_L-t)\times(N_S+N_L)}$ and $\widetilde{\boldsymbol{B}} \in \mathbb{R}^{(N_S+N_L)\times(N_S+N_L-t)}$ between the charge coefficient vector and reduced charge coefficient vector can be defined as

$$\boldsymbol{\rho}_r = \widetilde{\boldsymbol{F}} \cdot \boldsymbol{\rho}, \quad \boldsymbol{\rho} = \widetilde{\boldsymbol{B}} \cdot \boldsymbol{\rho}_r. \tag{20}$$

After applying charge neutrality constraint, the reduced formulation of DG-AEFIE can be written as

$$\begin{bmatrix} \widetilde{\boldsymbol{V}} & \widetilde{\boldsymbol{D}}^T \cdot \widetilde{\boldsymbol{P}} \cdot \widetilde{\boldsymbol{B}} \\ \widetilde{\boldsymbol{F}} \cdot \widetilde{\boldsymbol{D}} & k_0^2 \widetilde{\boldsymbol{I}}_r \end{bmatrix} \cdot \begin{bmatrix} jk_0 \boldsymbol{j} \\ c_0 \boldsymbol{\rho}_r \end{bmatrix} = \begin{bmatrix} \eta_0^{-1} \boldsymbol{b} \\ \boldsymbol{0} \end{bmatrix} \tag{21}$$

in which $\widetilde{\boldsymbol{I}}_r \in \mathbb{R}^{(N_S+N_L-t)\times(N_S+N_L-t)}$ is an identity matrix. The conditioning of the proposed DG-AEFIE is stable over wide frequencies without imbalance between the vector potential and scalar potential. In addition, the DG-AEFIE provides an easy way to analyze the multiscale structure at low frequencies with both conformal and nonconformal meshes.

B. Perturbation Method for DG-AEFIE

The DG-AEFIE loses accuracy of current for plane electromagnetic scattering problems at extremely low frequencies. In order to remedy the low-frequency inaccuracy problems, the perturbation method [26], [30] is incorporated into DG-AEFIE. When the operation frequency is extremely low ($|k_0 R| \ll 1$), the Green's function can be approximated as

$$G(\boldsymbol{r}, \boldsymbol{r}') \approx \frac{1}{4\pi R}\left[1 + (-jk_0 R) + \frac{1}{2}(-jk_0 R)^2\right] \tag{22}$$

where the truncation error for $e^{-jk_0 R}$ is $\{(-jk_0 R)^3/6 + O((-jk_0 R)^4)\}$. The second order is enough in our work if $|k_0 R_{\max}|^3/6 < 1 \times 10^{-7}$ [30]. By expanding the Green's function in the DG-AEFIE, we have

$$\widetilde{\boldsymbol{V}} = \widetilde{\boldsymbol{V}}^{(0)} + \delta\widetilde{\boldsymbol{V}}^{(1)} + \delta^2\widetilde{\boldsymbol{V}}^{(2)} + O(\delta^3) \tag{23}$$

$$\widetilde{\boldsymbol{P}} = \widetilde{\boldsymbol{P}}^{(0)} + \delta\widetilde{\boldsymbol{P}}^{(1)} + \delta^2\widetilde{\boldsymbol{P}}^{(2)} + O(\delta^3) \tag{24}$$

$$\boldsymbol{b} = \boldsymbol{b}^{(0)} + \delta\boldsymbol{b}^{(1)} + \delta^2\boldsymbol{b}^{(2)} + O(\delta^3) \tag{25}$$

$$\boldsymbol{j} = \boldsymbol{j}^{(0)} + \delta\boldsymbol{j}^{(1)} + \delta^2\boldsymbol{j}^{(2)} + O(\delta^3) \tag{26}$$

$$\boldsymbol{\rho}_r = \boldsymbol{\rho}_r^{(0)} + \delta\boldsymbol{\rho}_r^{(1)} + \delta^2\boldsymbol{\rho}_r^{(2)} + O(\delta^3) \tag{27}$$

in which $\delta = -jk_0$. At low frequencies, $\widetilde{\boldsymbol{V}} \approx \widetilde{\boldsymbol{V}}^{(0)}$ and $\widetilde{\boldsymbol{P}} \approx \widetilde{\boldsymbol{P}}^{(0)}$ because the zeroth-order Green's function is the original form of Green's function in static regime. The different order of matrix $\widetilde{\boldsymbol{V}}$ and vector $\widetilde{\boldsymbol{b}}$ can be found in [26]. It should be noted that the matrix $\widetilde{\boldsymbol{P}}$ is different from that in [26] since we choose line charge basis functions in our method. In the matrix $\widetilde{\boldsymbol{P}}$, the expansion of the submatrix $\overline{\boldsymbol{P}}^{\mathrm{SS}}$, $\overline{\boldsymbol{P}}^{\mathrm{SL}}$, and $\overline{\boldsymbol{P}}^{\mathrm{LS}}$ can be easily obtained by replacing the Green's function using (22). For the line-line scalar potential, we have

$$\widetilde{\boldsymbol{P}}^{\mathrm{LL}(0)} = \widetilde{\boldsymbol{P}} \tag{28}$$

$$\widetilde{\boldsymbol{P}}^{\mathrm{LL}(1)} = \overline{\boldsymbol{0}} \tag{29}$$

$$\widetilde{\boldsymbol{P}}^{\mathrm{LL}(2)} = \overline{\boldsymbol{0}}. \tag{30}$$

It is obvious that all the matrices and vectors are frequency independent. The different order of the solution of current and charge can be obtained accurately in a recursive style [26], [30].

C. Preconditioning for DG-AEFIE

Even the conditioning of the DG-AEFIE and DG-AEFIE with perturbation maintains stable when the frequency varies from the low frequency to the high frequency, the number of iterations is not so satisfactory. Inspired by the work in [25] and [31], a block matrix preconditioner can be incorporated into the proposed method to improve the iteration. The preconditioned linear discretized system is

$$\overline{\boldsymbol{Z}} \cdot \overline{\boldsymbol{\mathcal{P}}}^{-1} \cdot \boldsymbol{I} = \boldsymbol{V}. \tag{31}$$

In (32), $\overline{\boldsymbol{Z}}$ denotes the impedance matrix of the DG-AEFIE in (29), and $\boldsymbol{I}$ and $\boldsymbol{V}$ represent the coefficient and excitation vectors, respectively. The impedance matrix $\overline{\boldsymbol{Z}}$ can be approximated by a sparse form as

$$\overline{\boldsymbol{P}} \approx \begin{bmatrix} \mathrm{diag}(\widetilde{\boldsymbol{V}}) & \widetilde{\boldsymbol{D}}^T \cdot \mathrm{diag}(\widetilde{\boldsymbol{P}}) \cdot \widetilde{\boldsymbol{B}} \\ \widetilde{\boldsymbol{F}} \cdot \widetilde{\boldsymbol{D}} & k_0^2 \widetilde{\boldsymbol{I}}_r \end{bmatrix} \tag{32}$$

and its inverse can be adopted as a preconditioner which can be written by

$$\overline{\boldsymbol{\mathcal{P}}}^{-1} = \begin{bmatrix} \overline{\boldsymbol{X}}^{-1} & \boldsymbol{0} \\ \boldsymbol{0} & \boldsymbol{0} \end{bmatrix} + \begin{bmatrix} -\overline{\boldsymbol{X}}^{-1} \cdot \overline{\boldsymbol{Y}} \\ \overline{\boldsymbol{I}}_r \end{bmatrix} \cdot \overline{\Delta}^{-1} \cdot \begin{bmatrix} -\overline{\boldsymbol{W}} \cdot \overline{\boldsymbol{X}}^{-1} & \overline{\boldsymbol{I}}_r \end{bmatrix} \tag{33}$$

where

$$\overline{\boldsymbol{X}} = \mathrm{diag}(\widetilde{\boldsymbol{V}}) \tag{34}$$

$$\overline{\boldsymbol{Y}} = \widetilde{\boldsymbol{D}}^T \cdot \mathrm{diag}(\widetilde{\boldsymbol{P}}) \cdot \widetilde{\boldsymbol{B}} \tag{35}$$

$$\overline{\boldsymbol{W}} = \widetilde{\boldsymbol{F}} \cdot \widetilde{\boldsymbol{D}} \tag{36}$$

$$\overline{\boldsymbol{\Delta}} = k_0^2 \overline{\boldsymbol{I}}_r - \overline{\boldsymbol{W}} \cdot \overline{\boldsymbol{X}}^{-1} \cdot \overline{\boldsymbol{Y}}. \tag{37}$$

Since the matrix $\overline{\boldsymbol{X}}$ is a diagonal matrix, its inverse can be easily obtained. For the preconditioner of DG-AEFIE with perturbation method, the matrix $\widetilde{\boldsymbol{V}}$ and $\widetilde{\boldsymbol{P}}$ in (33) are replaced by their zero-order forms.

III. Numerical Results

In this section, the proposed method is demonstrated by several numerical examples. At first, the electromagnetic scattering from a PEC sphere was analyzed with conformal mesh using the proposed method. It was followed by the analysis of a cone divided into three parts where the mesh was locally refined. Finally, the proposed method was used to compute the scattering problems of a PEC chip and a complicated ship model with nonconformal mesh. Assume that a plane wave with amplitude of 1 V/m illuminates on the scatters along the $-z$ axis. In this paper, a Krylov subspace iterative method, GMRES [32] with a restart of 30, was chosen to solve the final linear system. We use a relative residual error ϵ of 10^{-8}.

A. Plane Wave Scattering From PEC Sphere

We first analyze the electromagnetic scattering from a PEC sphere with radius 0.5 m. The sphere was discretized into a conformal mesh with 1458 triangles. In the view of domain decomposition concept, the conformal discretization can be regarded as that the sphere is discretized into 1458 subdomains

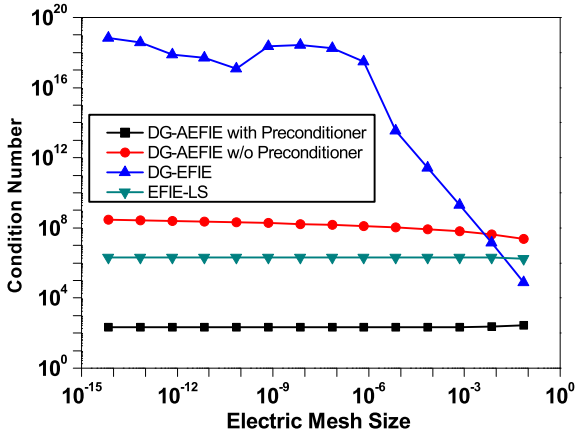

Fig. 3. Condition number of the impedance matrices of DG-AEFIE with/without preconditioner, DG-EFIE, and EFIE-LS as electric size varies.

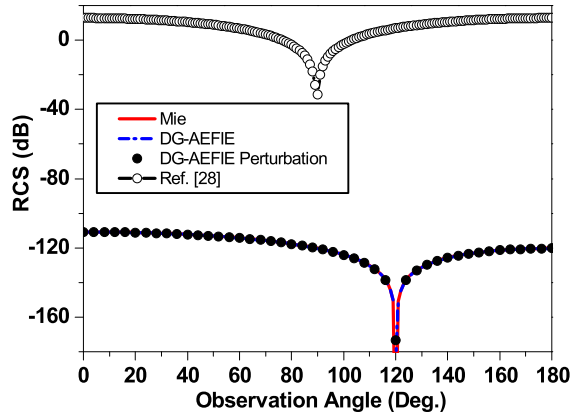

Fig. 4. Comparison of the RCS of a PEC sphere at 10^5 Hz (electric mesh size: 2.37×10^{-5}). The RCS results are computed by DG-AEFIE, DG-AEFIE with perturbation method, and the algorithm in [28]. The reference solution is calculated by the Mie series.

and 4374 interface contour edges between two adjacent subdomains. Since there is only one triangle in each subdomain, three half RWG basis functions are defined on every subdomain. Consequently, 4374 half RWG basis functions were used to expand the surface current, 1458 surface charge basis functions, and 4374 line charge bases are chosen to expand the charge. In order to estimate the accuracy of the result, we define the relative error as $20\log(||\boldsymbol{R}_1 - \boldsymbol{R}_0||_2/||\boldsymbol{R}_0||_2)$. Here, $||\cdot||_2$ means 2-norm, and $\boldsymbol{R}_0$ and $\boldsymbol{R}_1$ denote the reference result and the result computed by the proposed method, respectively.

We first examine the condition number of the impedance matrices of DG-AEFIE with/without preconditioner, DG-EFIE, EFIE-LS, and the proposed method in [28] over a very wide frequency band and the electric mesh size (h/λ) ranges from 7.10×10^{-15} to 7.10×10^{-2}. In Fig. 3, it is apparent that the system matrices of DG-AEFIE with/without preconditioner and EFIE-LS almost have a constant conditioner number over frequencies while the condition number of DG-EFIE increases as the electric size decreases. Obviously, the conditioning of DG-AEFIE with preconditioner is better than the other three ones.

Fig. 4 shows the far-field RCS at $\theta = [0°, 180°]$ calculated by the proposed method at 10^5 Hz. From the results, it can be

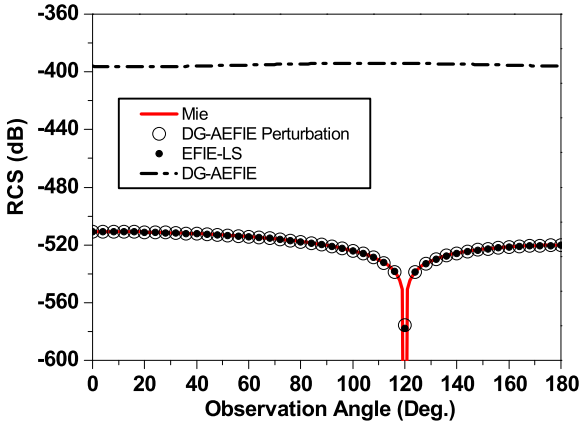

Fig. 5. Comparison of the RCS of a PEC sphere at 3×10^{-5} Hz (electric mesh size: 7.10×10^{-15}). The RCS data are computed by DG-AEFIE with perturbation method, EFIE with LS basis functions, DG-EFIE, and DG-AEFIE. The reference solution is calculated by the Mie series.

TABLE I
RELATIVE ERROR OF THE SURFACE CURRENT

Electric mesh Size	DG-AEFIE			DG-AEFIE Perturbation		
	α_1	α_2	α_3	α_1	α_2	α_3
7.10×10^{-5}	-104.4	-104.4	-104.3	-5.6	-25.0	-49.4
7.10×10^{-7}	-70.0	-79.3	-78.5	-5.6	-28.4	-52.0
7.10×10^{-9}	-16.7	-14.5	-15.1	-5.6	-31.8	-54.3
7.10×10^{-12}	29.0	18.8	18.1	-5.6	-33.5	-55.4
7.10×10^{-15}	81.0	83.5	82.4	-5.6	-35.4	-56.6

found that both the DG-AEFIE and DG-AEFIE with perturbation method have no breakdown and inaccuracy problems. However, the result calculated by the method in [28] is not correct. Fig. 5 compares the RCS data at 3×10^{-5} Hz. The results calculated by DG-AEFIE with perturbation method and EFIE-LS agree well with the Mie series solution. However, the result of DG-AEFIE without perturbation method is wrong due to the low-frequency inaccuracy of current.

The relative error of the surface current calculated by using DG-AEFIE with/without perturbation method is shown in Table I. The stabilization parameter α was chosen to be $\alpha_1(= 0.1)$, $\alpha_2(= 1)$, and $\alpha_3(= 20\log(\lambda/h))$. From Table I, it can be seen that the relative error of DG-AEFIE without perturbation method becomes larger when the electric size decreases. However, the DG-AEFIE with perturbation method is accurate even at extremely low frequency. Among α_1, α_2, and α_3, the result of DG-AEFIE with perturbation method is the most accurate when $\alpha = \alpha_3$.

B. Plane Wave Scattering From PEC Cone

In this numerical example, a PEC cone target was analyzed. The height and base radius of the cone are 1.5 and 0.6 m, respectively. As shown in Fig. 6, the cone was decomposed into three sections, and every section was discretized with different mesh size independently. The final generated mesh is nonconformal. The average mesh size of each part is 0.1543, 0.0498, and 0.0126 m. There are 4064 triangles and 6068 inner edges in the top subdo-

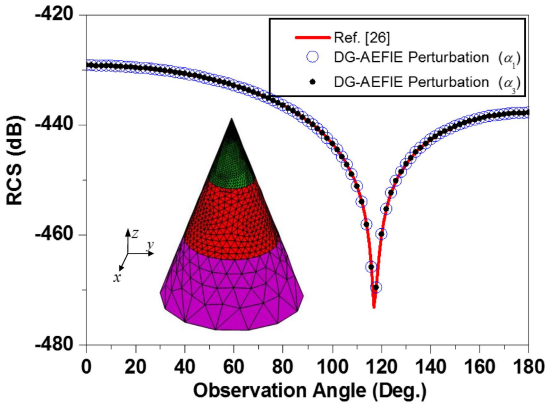

Fig. 6. Comparison of the RCS of a PEC cone at 10^{-3} Hz. The RCS results are computed by DG-AEFIE with perturbation method, and the stabilization parameter is α_1 and α_3. The reference result is obtained by the method in [26] with conformal mesh.

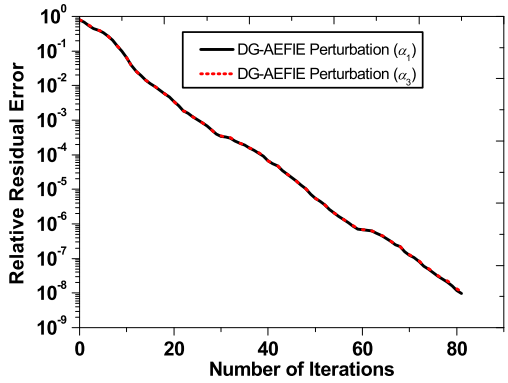

Fig. 7. Convergence history of the DG-AEFIE with perturbation method at 10^{-3} Hz.

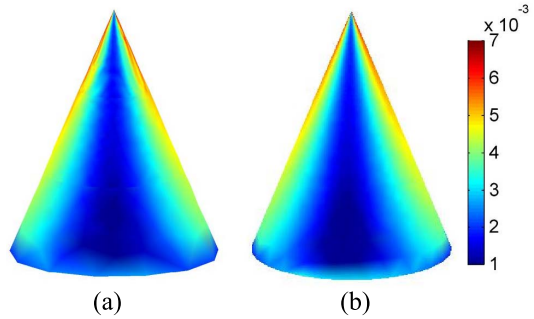

Fig. 8. Surface current distributions of PEC cone at 10^{-3} Hz. (a) DG-AEFIE with perturbation method. (b) EFIE-LS (conformal mesh).

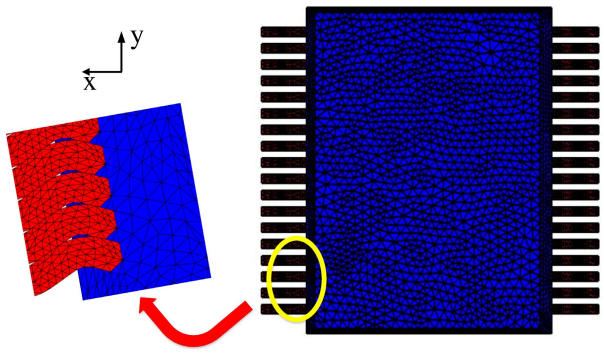

Fig. 9. Nonconformal mesh of a PEC chip.

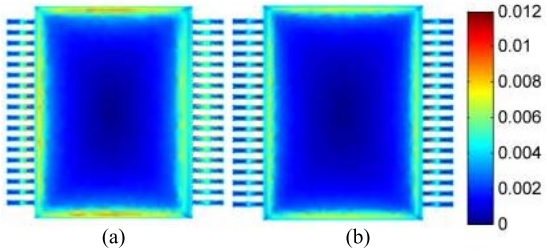

Fig. 10. Surface current distribution of the PEC chip at 1 Hz. (a) DG-AEFIE with perturbation method. (b) EFIF-LS (conformal mesh).

domain, and 240 triangles and 349 inner edges in the bottom subdomain. Totally, 7833 RWGs, 150 half RWGs, 5272 surface charge bases, and 100 line charge bases were generated. Fig. 6 shows the RCS of the PEC cone at 10^{-3} Hz. The result calculated by DG-AEFIE with perturbation method is practically identical to the reference solution when the stabilization parameter is α_1 and α_3. Shown in Fig. 7 is the convergence history of the DG-AEFIE with perturbation method when the stabilization parameter is α_1 and α_3. The iteration step required for convergence associated with the two stabilization parameters almost equal to each other. From Figs. 6 and 7, it can be seen that the accuracy and convergence of the DG-AEFIE with perturbation method is not sensitive to the choice of the stabilization parameter when the mesh is nonconformal. Fig. 8 shows the surface current distributions of the PEC cone at 10^{-3} Hz. The result obtained by DG-AEFIE with perturbation method agrees well with EFIE-LS.

C. Plane Wave Scattering From PEC Chip

In the third numerical example, a PEC chip was analyzed. In Fig. 9, the chip lies in the yz plane and the x-axis is perpendicular to the paper. There are 18 legs with distance of 0.027 cm between each other at left and right sides of the chip, respectively. The length of chip along the z-direction is 1 cm, while 1.034 cm along the y-direction. The chip was divided into two parts. The first part is the main body (blue in Fig. 9) of the chip, and the second part consists of 36 legs (red in Fig. 9). The two parts were discretized independently. It is obvious that the mesh along the contour between main body and every leg is nonconformal in Fig. 9. In the mesh of main body, there are 6950 triangles and 10 353 inner edges. Each leg of the chip was discretized into 340 triangles and 506 inner edges. Consequently, in the final DG-AEFIE system, there are 28 569 RWGs, 432 half RWGs, 19 190 surface charge basis functions, and 288 line charge basis functions.

Fig. 10 shows the surface current distributions of the PEC chip at 1 Hz. The results were calculated by DG-AEFIE with perturbation method and EFIE-LS with conformal mesh. As can be seen from Fig. 10, the current distributions are alike without noticeable differences between the two results.

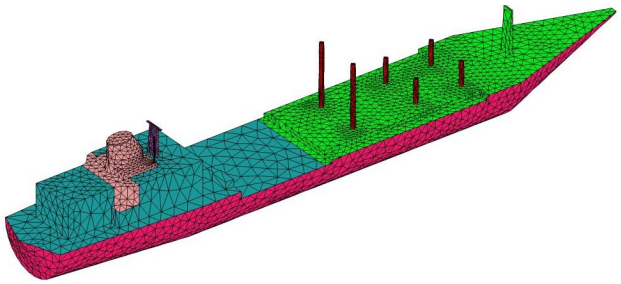

Fig. 11. Nonconformal mesh of a PEC ship.

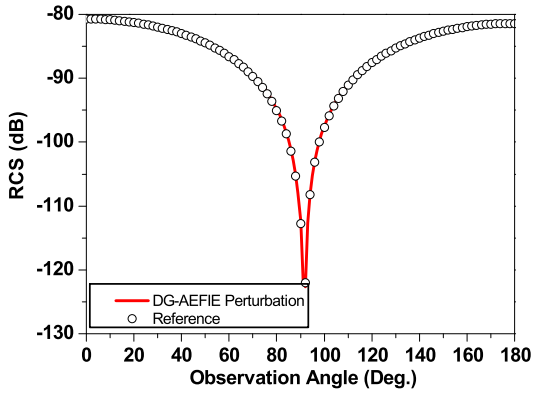

Fig. 12. Comparison of the RCS of a PEC ship at 10^3 Hz. The RCS data are computed by DG-AEFIE with perturbation method and EFIE-LS (conformal mesh).

It took 107 steps to convergence for DG-AEFIE with perturbation method, while EFIE-LS could not converge even after 10 000 steps.

D. Plane Wave Scattering From PEC Ship

At the last example, the low-frequency electromagnetic scattering from the PEC ship was analyzed. As shown in Fig. 11, the PEC ship was decomposed into seven parts in different colors. The large platform comprises several fine structures and components. The ratio of the maximum edge length versus the minimum edge length is 594.84, much larger than the above examples. The RCS was computed and compared against the one that was obtained by fully conformal meshes using EFIE-LS. A good agreement of the RCS is shown in Fig. 12. It took 208 steps for the DG-AEFIE with perturbation method to converge. Since DG-AEFIE is efficient to handle nonconformal meshes, we can generate the fine meshes for the thin structures to capture the geometry feature and coarse mesh for the platform at the low frequencies, and locally refine the mesh of the platform at the high frequencies with great flexibility.

IV. Conclusion

The DG-AEIF formulation is presented in this paper. It combines the domain decomposition method based on DG with AEFIE formulation. The transmission condition between adjacent subdomains is enforced with the aid of DG. Inheriting the well-conditioned advantage of the AEFIE, the proposed method converges fast over wide frequency band after preconditioning. In addition, it is efficient to analyze the multiscale targets by using nonconformal discretization with great flexibility. The numerical examples demonstrate the excellent performance of the proposed method.

References

[1] S. M. Rao, D. R. Wilton, and A. W. Glisson, "Electromagnetic scattering by surfaces of arbitrary shape," *IEEE Trans. Antennas Propag.*, vol. 30, no. 3, pp. 409–418, May 1982.

[2] Z. G. Qian and W. C. Chew, "Fast full-wave surface integral equation solver for multiscale structure modeling," *IEEE Trans. Antennas Propag.*, vol. 57, no. 11, pp. 3594–3601, Nov. 2009.

[3] J. C. Young, Y. Xu, R. J. Adams, and S. D. Gedney, "High-order Nyström implementation of an augmented electric field integral equation," *IEEE Antennas Wireless Propag. Lett.*, vol. 11, pp. 846–849, Jul. 2012.

[4] J.-S. Zhao and W. C. Chew, "Integral equation solution of Maxwell's equations from zero frequency to microwave frequencies," *IEEE Trans. Antennas Propag.*, vol. 48, no. 10, pp. 1635–1645, Oct. 2000.

[5] M. A. E. Bautista, F. Vipiana, M. A. Francavilla, J. A. T. Vasquez, and G. Vecchi, "A nonconformal domain decomposition scheme for the analysis of multiscale structures," *IEEE Trans. Antennas Propag.*, vol. 63, no. 8, pp. 3548–3560, Aug. 2015.

[6] Z. Peng, X.-C. Wang, and J.-F. Lee, "Integral equation based domain decomposition method for solving electromagnetic wave scattering from non-penetrable objects," *IEEE Trans. Antennas Propag.*, vol. 59, no. 9, pp. 3328–3338, Sep. 2011.

[7] K. Zhao, V. Rawat, S. C. Lee, and J. F. Lee, "A domain decomposition method with nonconformal meshes for finite periodic and semi-periodic structures," *IEEE Trans. Antennas Propag.*, vol. 55, no. 9, pp. 2559–2570, Sep. 2007.

[8] D. N. Arnold, F. Brezzi, B. Cockburn, and L. D. Marini, "Unified analysis of discontinuous Galerkin methods for elliptic problems," *SIAM J. Numer. Anal.*, vol. 39, no. 5, pp. 1749–1779, 2002.

[9] B. Cockburn, J. Gopalakrishnan, and R. Lazarov, "Unified hybridization of discontinuous Galerkin, mixed, and continuous Galerkin methods for second order elliptic problems," *SIAM J. Numer. Anal.*, vol. 47, no. 2, pp. 1319–1365, 2009.

[10] B. Cockburn, G. E. Karniadakis, and C.-W. Shu, *Discontinuous Galerkin Methods: Theory, Computation and Applications*. Tokyo, Japan: Springer-Verlag, 2000.

[11] J. Alvarez, L. D. Angulo, M. F. Pantoja, A. R. Bretones, and S. G. Garcia, "Source and boundary implementation in vector and scalar DGTD," *IEEE Trans. Antennas Propag.*, vol. 58, no. 6, pp. 1997–2003, Jun. 2010.

[12] P. Li, Y. Shi, L. J. Jiang, and H. Bagci, "A hybrid time-domain discontinuous Galerkin-boundary integral method for electromagnetic scattering analysis," *IEEE Trans. Antennas Propag.*, vol. 62, no. 5, pp. 2841–2846, May 2014.

[13] P. Li, Y. Shi, L. J. Jiang, and H. Bağcı, "DGTD analysis of electromagnetic scattering from penetrable conductive objects with IBC," *IEEE Trans. Antennas Propag.*, vol. 63, no. 12, pp. 5686–5697, Dec. 2015.

[14] S. Dosopoulos and J. F. Lee, "Interconnect and lumped elements modeling in interior penalty discontinuous Galerkin time-domain methods," *J. Comput. Phys.*, vol. 229, pp. 8521–8536, Aug. 2010.

[15] S. Dosopoulos, B. Zhao, and J.-F. Lee, "Non-conformal and parallel discontinuous Galerkin time domain method for Maxwell's equations: EM analysis of IC packages," *J. Comput. Phys.*, vol. 238, pp. 48–70, Apr. 2013.

[16] P. Li and L. J. Jiang, "Integration of arbitrary lumped multiport circuit networks into the discontinuous Galerkin time-domain analysis," *IEEE Trans. Microw. Theory Techn.*, vol. 61, no. 7, pp. 2525–2534, Jul. 2013.

[17] Z. Peng, K.-H. Lim, and J.-F. Lee, "A discontinuous Galerkin surface integral equation method for electromagnetic wave scattering from nonpenetrable targets," *IEEE Trans. Antennas Propag.*, vol. 61, no. 7, pp. 3617–3628, Jul. 2013.

[18] G. Xiao and Y. Hou, "Intuitive formulation of discontinuous Galerkin surface integral equations for electromagnetic scattering problems," *IEEE Trans. Antennas Propag.*, vol. 65, no. 1, pp. 287–294, Jan. 2017.

[19] G. Vecchi, "Loop-star decomposition of basis functions in the discretization of the EFIE," *IEEE Trans. Antennas Propag.*, vol. 47, no. 2, pp. 339–346, Feb. 1999.

[20] J.-F. Lee, R. Lee, and R. J. Burkholder, "Loop star basis functions and a robust preconditioner for EFIE scattering problems," *IEEE Trans. Antennas Propag.*, vol. 51, no. 8, pp. 1855–1863, Aug. 2003.
[21] S. Yan, J.-M. Jin, and Z. Nie, "EFIE analysis of low-frequency problems with loop-star decomposition and Calderón multiplicative preconditioner," *IEEE Trans. Antennas Propag.*, vol. 58, no. 3, pp. 857–867, Mar. 2010.
[22] F. P. Andriulli and G. Vecchi, "A Helmholtz-stable fast solution of the electric field integral equation," *IEEE Trans. Antennas Propag.*, vol. 60, no. 5, pp. 2357–2366, May 2012.
[23] F. P. Andriulli, F. Vipiana, and G. Vecchi, "Hierarchical bases for nonhierarchic 3-D triangular meshes," *IEEE Trans. Antennas Propag.*, vol. 56, no. 8, pp. 2288–2297, Aug. 2008.
[24] F. Vipiana, P. Pirinoli, and G. Vecchi, "A multiresolution method of moments for triangular meshes," *IEEE Trans. Antennas Propag.*, vol. 53, no. 7, pp. 2247–2258, Jul. 2005.
[25] T. Xia *et al.*, "An enhanced augmented electric-field integral equation formulation for dielectric objects," *IEEE Trans. Antennas Propag.*, vol. 64, no. 6, pp. 2339–2347, Jun. 2016.
[26] Z.-G. Qian and W. C. Chew, "Enhanced A-EFIE with perturbation method," *IEEE Trans. Antennas Propag.*, vol. 58, no. 10, pp. 3256–3264, Oct. 2010.
[27] X. Tian and G. Xiao, "Time-domain augmented electric field integral equation for a robust marching on in time solver," *IET Microw., Antennas Propag.*, vol. 8, no. 9, pp. 688–694, Jun. 2014.
[28] K.-J. Xu, X.-M. Pan, and X.-Q. Sheng, "An augmented EFIE with discontinuous Galerkin discretization," in *Proc. IEEE Int. Conf. Comput. Electromagn. (ICCEM)*, Feb. 2016, pp. 106–108.
[29] Z. Peng, R. Hiptmair, Y. Shao, and B. MacKie-Mason, "Domain decomposition preconditioning for surface integral equations in solving challenging electromagnetic scattering problems," *IEEE Trans. Antennas Propag.*, vol. 64, no. 1, pp. 210–223, Jan. 2016.
[30] S. Sun, Y. G. Liu, W. C. Chew, and Z. Ma, "Calderón multiplicative preconditioned EFIE with perturbation method," *IEEE Trans. Antennas Propag.*, vol. 61, no. 1, pp. 247–255, Jan. 2013.
[31] J.-H. Yeom, H. Chin, H.-T. Kim, and K.-T. Kim, "Block matrix preconditioner method for the electric field integral equation (EFIE) formulation based on loop-star basis functions," *Prog. Electromagn. Res.*, vol. 134, pp. 543–558, 2013.
[32] Y. Saad and M. H. Schultz, "GMRES: A generalized minimal residual algorithm for solving nonsymmetric linear systems," *SIAM J. Sci. Statist. Comput.*, vol. 7, no. 3, pp. 856–869, 1986.

Yibei Hou (S'15) received the B.S. degree from the University of Electronic Science and Technology of China, Chengdu, China, in 2014. He is currently pursuing the Ph.D. degree in electronic engineering with Shanghai Jiao Tong University, Shanghai, China.

His current research interests include computational electromagnetics and its application in scattering and radiation problems.

Gaobiao Xiao (M'10) received the B.S. degree from the Huazhong University of Science and Technology, Wuhan, China, in 1988, the M.S. degree from the National University of Defense Technology, Changsha, China, in 1991, and the Ph.D. degree from Chiba University, Chiba, Japan, in 2002.

He was with Hunan University, Changsha, from 1991 to 1997. Since 2004, he has been a Faculty Member with the Department of Electronic Engineering, Shanghai Jiao Tong University, Shanghai, China. His current research interests include numerical methods in electromagnetic fields, coupled thermoelectromagnetic analysis, microwave filter designs, fiber-optic filter designs, phased arrays, and inverse scattering problems.

Xuezhe Tian (S'12–M'17) received the B.S. degree from Harbin Engineering University, Harbin, China, in 2011, and the Ph.D. degree in electronic engineering from Shanghai Jiao Tong University, Shanghai, China, in 2016.

Since 2016, he has been a Post-Doctoral Researcher with the ElectroScience Laboratory, Ohio State University, Columbus, OH, USA. His current research interests include scientific computing, focusing on the computational electromagnetics and its application in various scattering and radiation problems, including the material modeling, SAR imaging, as well as EMC/EMI analysis.